J. Phase Equilib. Diffus. (2018) 39:750–765
https://doi.org/10.1007/s11669-018-0665-9

The Isothermal Section of the Phase Diagram of Dy-Sm-Ge Ternary System at 873 K

Z. Shpyrka[1] · K. Kluziak[2] · B. Rożdżyńska-Kiełbik[2] · A. Stetskiv[3] · V. Pavlyuk[1,2]

Submitted: 12 February 2018 / in revised form: 11 July 2018 / Published online: 9 August 2018

Abstract The interaction of components in the Dy-Sm-Ge system at 873 K was investigated by means of x-ray phase and structural analyses, microstructural analysis and energy dispersive x-ray spectroscopy. The existence of the continuous solid solutions between the isostructural binary germanides of the $Dy_{1-x}Sm_xGe$ (CrB-type), $Dy_{5-x}Sm_xGe_4$ (Sm_5Ge_4-type) and $Dy_{5-x}Sm_xGe_3$ (Mn_5Si_3-type) were established. The limited solid solutions based on the binary germanides of the $SmGe_2$ (α-$ThSi_2$-type), $DyGe_2$ ($TbGe_2$-type) and $Dy_{11}Ge_{10}$ ($Ho_{11}Ge_{10}$-type) are formed. The solubility of Dy in $SmGe_2$ is 15 at.%, Sm in $DyGe_2$ and $Dy_{11}Ge_{10}$ − 10 at.%, Sm. Two ternary $Sm_xDy_{1-x}Ge_{1.5}$ (x = 0.15-0.50) and $Sm_2Dy_2Ge_7$ compounds were found. $Sm_xDy_{1-x}Ge_{1.5}$ crystallizes in AlB_2 structure type. The crystal structure of the new ternary compound of the $Sm_2Dy_2Ge_7$ (ordered superstructure to Nd_4Ge_7-type, Pearson symbol *oS*44, space group $C222_1$, a = 0.5942(1), b = 1.3823(4), c = 1.1801(3) nm, V = 0.9694 nm^3) was investigated by means of x-ray single crystal diffraction. The germanium atoms form 3D anionic network the existence of which was confirmed by electronic structure calculations.

Keywords Dy-Sm-Ge · isothermal section · phase diagram · solid solution · intermetallics · crystal structure

1 Introduction

Rare-earth intermetallics have been extensively studied in different fields and applications, including magnetic materials, thermoelectric, hydrogen storage materials and other.[1,2] The development of new materials on the base of rare-earth metals alloys requires systematic investigation of interactions between the components in binary, ternary and multicomponent systems, construction of their phase diagrams, and determination of crystal structure of the obtained phases.

In literature there are experimental data on ternary R-R'-Ge systems, where R and R'—rare earth metals cerium or yttrium subgroups. The most detailed were studied the sections between digermanides RGe_2-$R'Ge_2$.[3] On these sections the solid solutions as well as individual ternary phases are formed. The continuous solid solution for $DyGe_2$-$TbGe_2$ section was observed. In the $DyGe_2$-RGe_2 (were R = Er, Ho, Tm and Lu) sections forms the limited solid solutions. In the ternary systems with dysprosium the intermetallic compounds $Dy_{0.67}Tm_{0.33}Ge_{1.85}$,[4] $Dy_{0.5}Ho_{0.5}Ge_{1.75}$[5] and $Dy_{0.6}Lu_{0.4}Ge_2$[6] were observed. In the systems with samarium only one ternary compound of $Sm_{0.625}Lu_{0.375}Ge_{1.85}$[7] was studied.

In this contribution we report experimental results of the investigation of isothermal section at 873 K of phase diagram of the Dy-Sm-Ge ternary system in full concentration range.

Electronic supplementary material The online version of this article (https://doi.org/10.1007/s11669-018-0665-9) contains supplementary material, which is available to authorized users.

✉ V. Pavlyuk
vpavlyuk2002@yahoo.com

[1] Department of Inorganic Chemistry, Ivan Franko National University of Lviv, Kyryla and Mefodiya str. 6, Lviv 79005, Ukraine

[2] Institute of Chemistry, Environmental Protection and Biotechnology, Jan Długosz University of Częstochowa, al. Armii Krajowej 13/15, 42200 Częstochowa, Poland

[3] Department of Chemistry, Ivano-Frankivsk National Medical University, Galyska Str. 2, Ivano-Frankivsk 76018, Ukraine

2 Literature Data on Boundary Binary Diagrams

2.1 Sm-Ge System

The Sm-Ge phase diagram (Fig. 1a) was critically assessed by Gokhale and Abbaschian[8] based on experimental data of Eremenko et al.[9] Five binary compounds Sm_5Ge_3, Sm_5Ge_4, SmGe, $SmGe_{1.5}$, $SmGe_2$ forms in the Sm-Ge binary system. Sm_5Ge_3 phase melts congruently at 1973 K. The Sm_5Ge_4, SmGe and Sm_2Ge_3 ($SmGe_{1.5}$) forms peritectically.

$SmGe_{1.5}$ (or Sm_2Ge_3) compound exists in three polymorphic modifications. The polymorphic transition α-$SmGe_{1.5}$ ↔ β-$SmGe_{1.5}$ occurs at 1018 K, and the β-$SmGe_{1.5}$ ↔ γ-$SmGe_{1.5}$ polymorphic transition is at 1358 K. The orthorhombic and hexagonal Sm_3Ge_5[10,11] phases are the α-$SmGe_{1.5}$ and β-$SmGe_{1.5}$ polymorphic modifications respectively.

The $SmGe_2$[12] compound according to the structural data has a composition of $SmGe_{1.63}$[9] and forms by peritectoid reaction.

The described earlier Sm_4Ge_7[13,14] and $SmGe_5$[15] compounds which are not observed on phase diagram,

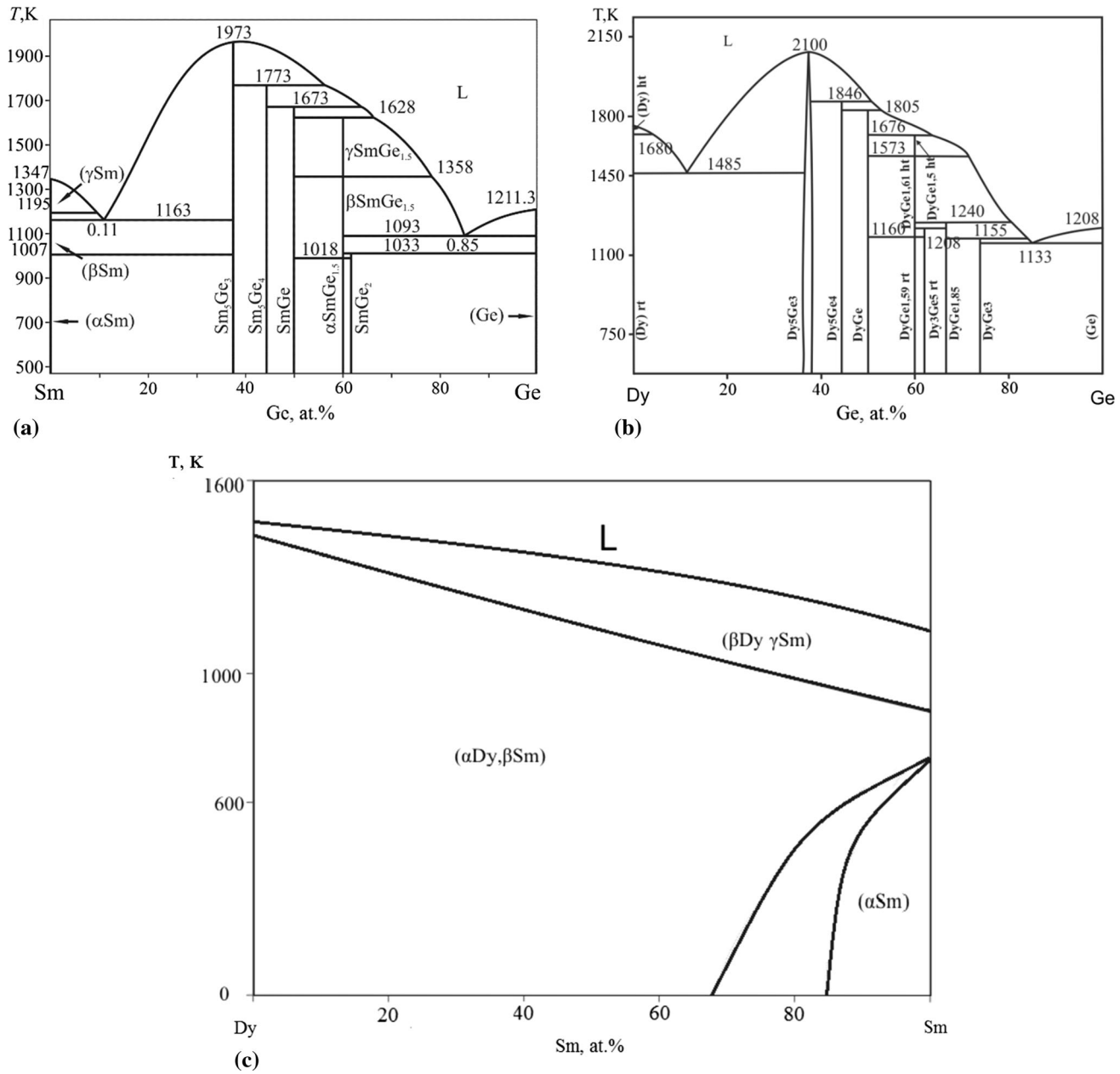

Fig. 1 Phase diagram of Sm-Ge (taken from Ref 8), Dy-Ge[17] and Dy-Sm[30] binary systems

probably, are metastable phases. Crystals of Sm_4Ge_7 was prepared by Zhang et al.[14] using the flux method, flux In (99.99 wt.%), heated to 1373 K at a rate of 300 K h^{-1}, heated at 1373 K for 1.5-3 h, cooled to 673 K over 20 h and structurally investigated by both x-ray and electron diffraction. This structure belongs to superstructure of RGe_{2-x} with the α-$ThSi_2$ or α-$GdSi_2$ types at x = 1/4. The orthorhombic structure is realized through the long-range order of vacant Ge positions. The high-pressure phase $SmGe_5$[15] synthesized by heating of pure elements at 1123 K and 10 GPa. New germanide Sm_2Ge_9 was received by thermal decomposition of high-pressure phase $SmGe_5$[16]

Crystallographic characteristics of all known Sm-Ge binary compounds are presented in Table 1.

2.2 Dy-Ge System

The Dy-Ge phase diagram (Fig. 1b) is redrawn from Eremenko et al.[17] Seven binary compounds: Dy_5Ge_3, Dy_5Ge_4, DyGe, $DyGe_{1.59}$ (Dy_2Ge_3), Dy_3Ge_5, $DyGe_{1.85}$ and $DyGe_3$ forms in this system.[18-26] The $DyGe_3$, $DyGe_{1.85}$, $DyGe_{1.59}$, DyGe and Dy_5Ge_4 phases are formed by peritectic reactions.

The polymorphic transitions α-$DyGe_{1.59}$ ↔ β-$DyGe_{1.61}$ and β-$DyGe_{1.61}$ ↔ γ-$DyGe_{1.5}$ at 1160 K and 1573 K are observed respectively. The reaction of formation of the Dy_3Ge_5 is peritectoid.

The Dy_5Ge_3 germanide melts congruently at 2100 K and has a has an insignificant ~2 at.% homogeneity region.

During the investigation of polymorphism in the binary rare-earth metal germanides the new hexagonal phase of Dy_3Ge_5 was observed at 120 K by Tobash et al.[27]

The $DyGe_{1.90}$, Dy_3Ge_4 (T = 20 K)[28] and $Dy_{11}Ge_{10}$[21] compounds for which crystal structures were studied, but are not displayed on the diagram.

New cubic phase $DyGe_{2.85}$ crystallized in the cubic $AuCu_3$ structure type was synthesized at a pressure of 8 GPa and described by Tsvyashchenko *et al.*[29]

Crystallographic characteristics of known Dy-Ge binary compounds are presented in Table 2.

2.3 Dy-Sm System

The Dy-Sm phase diagram (Fig. 1b) is redrawn from Okamoto.[30] Dysprosium exists in two allotropic modifications: α-Dy (Mg-type) and β-Dy (W-type). The transformation α-Dy ↔ β-Dy occurs at 1654 K. Samarium exists in three allotropic modifications: α-Sm (Sm-type), β-Sm (Mg-type) and γ-Sm (W-type). The transformation of α-Sm to β-Sm occurs at 1007 K and the following transformation of β-Sm ↔ γ-Sm is at 1195 K.

Based on the high-temperature modifications β-Dy and γ-Sm and low-temperature modifications α-Dy and β-Sm forms continuous series of solid solutions (β-Dy/γ-Sm and α-Dy/β-Sm). Based on low-temperature modifications of α-Sm limited solid solution is formed, and the homogeneity region of which extends from 15 to 25 at.% Dy at room temperature.

3 Experimental Details

Samarium, dysprosium and germanium, all with a nominal purity greater than 99.9 wt.%, were used as starting materials. The 64 samples a total mass of each about 2 g

Table 1 Literature data for binary phases of the Sm-Ge system

Phase	Structure type	Pearson symbol	Space group	Unit cell dimensions, nm			Ref
				a	*b*	*c*	
Sm_5Ge_3	Mn_5Si_3	*hP*16	$P6_3/mcm$	0.866	…	0.649	9
Sm_5Ge_4	Sm_5Ge_4	*oP*36	*Pnma*	0.774	1.495	0.784	9
SmGe	CrB	*oS*8	*Cmcm*	0.436	1.086	0.401	9
Sm_3Ge_5 (α-$SmGe_{1.5}$)	Sm_3Ge_5	*hP*16	*P*-62*c*	0.69238	…	0.8491	10,11
Sm_3Ge_5 (β-$SmGe_{1.5}$)	Y_3Ge_5	*oF*64	*Fdd*2	0.58281	1.7476	1.3875	10,11
γ-$SmGe_{1.5}$	AlB_2	*hP*3	*P*6/*mmm*	0.4005	…	0.4250	9
$SmGe_2$ ($SmGe_{1.63-1.73}$)	α-$ThSi_2$	*tI*12	$I4_1/amd$	0.412	…	1.396	9,12,13
$SmGe_{1.73}$	$GdSi_{1.4}$	*oI*12	*Imma*	0.41636	0.41643	1.3773	13
Sm_4Ge_7	Nd_4Ge_7	*oS*44	$C222_1$	0.5890	1.3836	1.1788	13,14
Sm_2Ge_9	Nd_2Ge_9	*oP*22	*Pmmn*	0.39546	0.9464	1.2321	16
$SmGe_5$	$SmGe_5$	*oI*12	*Immm*	0.39805	0.61522	0.9839	15

Table 2 Literature data for binary phases of the Dy-Ge system

Phase	Structure type	Pearson symbol	Space group	Unit cel dimensions, nm			Ref
				a	*b*	*c*	
Dy_5Ge_3	Mn_5Si_3	*hP*16	$P6_3/mcm$	0.844	…	0.633	18
Dy_5Ge_4	Sm_5Ge_4	*oP*36	Pnma	0.758	1.454	0.765	19
$Dy_{11}Ge_{10}$	$Ho_{11}Ge_{10}$	*tI*84	*I4/mmm*	1.081	…	1.629	20
DyGe	CrB	*oS*8	Cmcm	0.4272	1.0678	0.3931	20
Dy_3Ge_4	Er_3Ge_4	*oS*28	*Cmcm*	0.4027	1.0599	1.4169	28
α-$DyGe_{1.59}$			*monoclinic*	0.3944	0.6800	0.4135	10
					β = 89.88		
β-$DyGe_{1.61}$	α-$ThSi_2$	*tI*12	$I4_1/amd$	0.4047	…	1.3716	21
γ-$DyGe_{1.5}$	AlB_2	*hP*3	P6/mmm	0.3920	…	0.4130	22
$Dy_{11}Ge_{18}$	$Dy_{11}Ge_{18}$	*oF*232	*Fdd2*	6.29970	1.3692	0.57159	23
Dy_3Ge_5	Y_3Ge_5	*oF*64	*Fdd2*	0.5729	1.7190	1.3678	25
Dy_3Ge_5 (120 K)	Dy_3Ge_5	*hP*16	*P*-62*c*	0.68387		0.8293	27
$DyGe_{1.85}$	$DyGe_{1,85}$	*oS*24	$Cmc2_1$	0.41027	2.9705	0.39316	24
$DyGe_{1,90}$	$TbGe_2$	*oS*24	*Cmmm*	0.4100	2.9753	0.4005	25
$DyGe_{2.85}$	$AuCu_3$	*cP*4	*Pm*-3*m*	0.4286			29
$DyGe_3$	$DyGe_3$	*oS*16	*Cmcm*	0.4042	2.072	0.3919	26

were prepared by arc melting of pure metals in a high-purity argon atmosphere. The mass losses after the melting were less than 1 wt.%. After the melting the samples were sealed in evacuated quartz ampoules and annealed at 873 K during 720 h. After annealing the ampoules with the samples were quenched in cold water.

Phase analysis of the samples was carried out with the use of powder x-ray diffraction (XRD) (DRON-4.0M and STOE STADI P diffractometers with Fe- and Cu-Kα radiation, respectively). The obtained powder diffraction data were analyzed by Rietveld method using Fullprof software.[31] Wavelength Dispersive Spectrometry (WDS) and CAMECA SX-100 Electron Probe Micro Analyser (EPMA) and REMMA-102-02 scanning microscope were used to measure the number of phases and their qualitative and quantitative chemical compositions some alloys.

Single crystal diffraction data were collected by Xcalibur^{TM}3 CCD diffractometer with graphite-monochromated Mo-Kα radiation. Scans were taken in the ω mode, the analytical absorption corrections were made by CrysalisRed[32] The crystal structure was solved by direct methods and refined using the SHELX-97 program package.[33,34]

The electronic structures of the ternary compound was calculated using the tight-binding linear muffin-tin orbital (TB-LMTO) method in the atomic spheres approximation (TB-LMTO-ASA[35–37]) using the experimental crystallographic data reported here. The exchange and correlation were interpreted in the local density approximation.[38] All the figures and graphics concerning electron structure calculations were generated using wxDragon.[39]

4 Results and Discussion

4.1 Isothermal Section at 873 K of the Dy-Sm-Ge System

The isothermal section of the Dy-Sm-Ge system at 873 K was constructed by XRD and SEM-EPMA methods based on the phase analysis of 13 binary and 51 ternary alloys (Fig. 2a, b). This isothermal section in the full concentration region consists of 11 three-phase, 23 two-phase and 13 single-phase regions. From Fig. 3(a)-(h), it can be seen that in the germanium-rich region at 870 K the stable phases are the $Dy_2Sm_2Ge_7$ ternary compound, solid solutions phases based on $SmGe_2$, $DyGe_{1.9}$ and $DyGe_3$ binary compounds. Formation of other binary phases known from the literature (metastable) or solid solutions based on these phases are not observed. The binary $SmGe_{2-x}$ phase with α-$ThSi_2$ structure type has homogeneity region from $SmGe_2$ to $SmGe_{1.67}$, although in the literature[9,12] for these compositions were indicated different structural types (α-$ThSi_2$ and AlB_2 respectively). From the $SmGe_{1.6}$ to $SmGe_{1.5}$ (α-$SmGe_{1.5}$) realized hexagonal Sm_3Ge_5 structure type.

The following three-phase regions were detected:

$Dy_{1-x}Sm_xGe_{1.9}$+ $Dy_{1-x}Sm_xGe_3$+Ge, $Dy_{1-x}Sm_xGe_{1.9}$+ $Dy_2Sm_2Ge_7$+Ge,

$Dy_{1-x}Sm_xGe_2$+ $Dy_2Sm_2Ge_7$+Ge, $Dy_{1-x}Sm_xGe_{1.9}$+ $Dy_2Sm_2Ge_7$+$Sm_xDy_{1-x}Ge_{1.5}$,

$Dy_xSm_{1-x}Ge_2$+ $Dy_2Sm_2Ge_7$+$Dy_{1-x}Sm_xGe_{1.5}$, $Sm_{1-x}Dy_xGe_2$+$Dy_{1-x}Sm_xGe$+$Dy_{1-x}Sm_xGe_{1.5}$,

$Dy_{5-x}Sm_xGe_4$+$Dy_{1-x}Sm_xGe$+$Dy_{11-x}Sm_xGe_{10}$, $Dy_{1-x}Sm_xGe_{1.9}$+$Dy_{1-x}Sm_xGe_{1.5}$+Dy_3Ge_5,

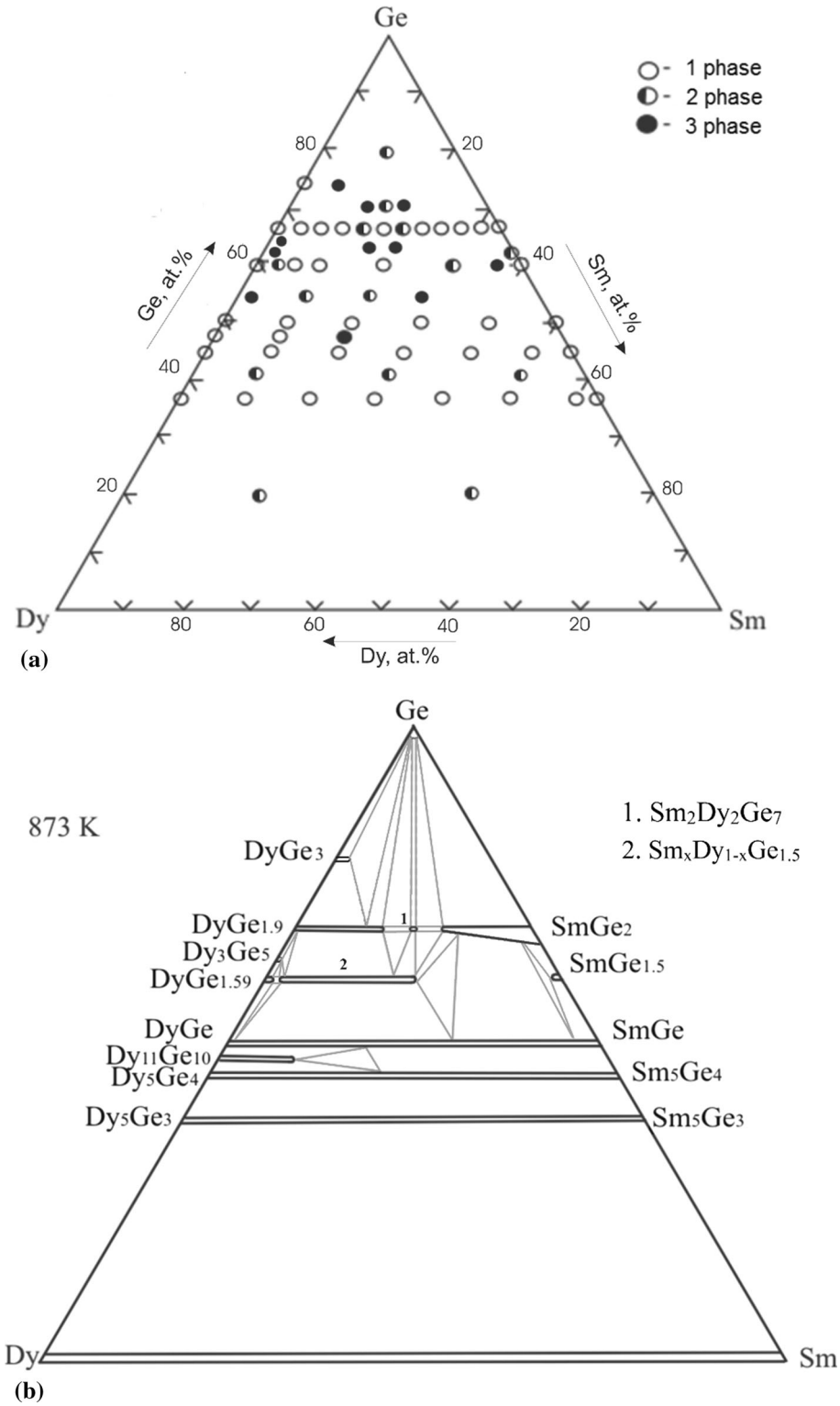

Fig. 2 Gross compositions of the analyzed Dy-Sm-Ge alloys (a) and isothermal section at 873 K (b)

$Dy_{1-x}Sm_xGe_{1.5}$+$DyGe_{1.59}$+Dy_3Ge_5, $Sm_xDy_{1-x}Ge_{1.5}$+ $DyGe_{1.59}$+ $Dy_{1-x}Sm_xGe$,

$Dy_xSm_{1-x}Ge_2$+$SmGe_{1.5}$+$Dy_{1-x}Sm_xGe$. The micrographs of selected three-phase samples are shown Fig. 4(a-f).

The single-phase regions consist new ternary compounds of $Dy_2Sm_2Ge_7$ and $Dy_{1-x}Sm_xGe_{1.5}$, limited solid solutions based on binary compounds: $Dy_{1-x}Sm_xGe_3$, $Dy_{1-x}Sm_xGe_{1.9}$, $Dy_xSm_{1-x}Ge_2$, $Dy_{11-x}Sm_xGe_{10}$ and continuous solid solutions: $Dy_{1-x}Sm_xGe$, $Dy_{5-x}Sm_xGe_4$ and

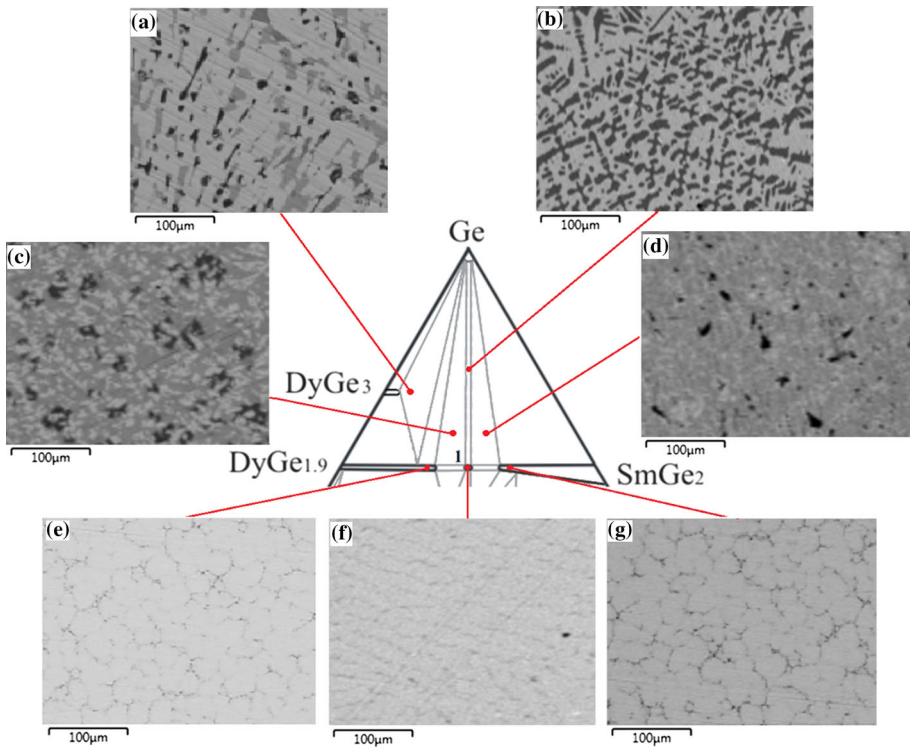

Fig. 3 Micrographs of selected samples from the Ge-rich region of Dy-Sm-Ge system: (a) $Dy_{20}Sm_5Ge_{75}$ (light grey phase—$Dy_{1-x}Sm_xGe_{1.9}$, composition from EPMA $Dy_{24.6(4)}Sm_{9.2(4)}Ge_{66.2(5)}$; grey phase—$Dy_xSm_{1-x}Ge_3$, $Dy_{20.1(3)}Sm_{4.8(3)}Ge_{75.1(4)}$; dark phase—Ge); (b) $Dy_{10}Sm_{10}Ge_{80}$ (grey phase—$Dy_2Sm_2Ge_7$, $Dy_{17.5(2)}Sm_{18.1(2)}Ge_{64.4(3)}$; dark phase—Ge); (c) $Dy_{18}Sm_{10}Ge_{72}$ (light grey phase—$Dy_{1-x}Sm_xGe_{1.9}$, $Dy_{23.1(3)}Sm_{10.6(3)}Ge_{66.3(4)}$; grey phase—$Dy_2Sm_2Ge_7$, $Dy_{17.7(2)}Sm_{18.1(2)}Ge_{64.2(3)}$; dark phase—Ge); (d) $Dy_{10}Sm_{18}Ge_{72}$ (light grey phase—$Dy_xSm_{1-x}Ge_2$, $Dy_{10.1(3)}Sm_{23.6(3)}Ge_{66.3(4)}$ grey phase—$Dy_2Sm_2Ge_7$, $Dy_{17.6(3)}Sm_{18.2(3)}Ge_{64.2(4)}$; dark phase—Ge); (e) $Dy_{24}Sm_{10}Ge_{66}$ (grey phase—$Dy_{1-x}Sm_xGe_{1.9}$, $Dy_{23.7(3)}Sm_{10.1(3)}Ge_{66.2(4)}$; single dark spots—Ge); (f) $Dy_{17}Sm_{17}Ge_{66}$ (grey phase—$Dy_2Sm_2Ge_7$, $Dy_{17.7(2)}Sm_{18.2(2)}Ge_{64.1(3)}$; single dark spots—Ge); (g) $Dy_{10}Sm_{24}Ge_{66}$ (grey phase—$Sm_{1-x}Dy_xGe_2$, $Dy_{10.7(2)}Sm_{22.9(3)}Ge_{66.4(4)}$; single dark spots—Ge)

$Dy_{5-x}Sm_xGe_3$. A solid solutions between the isostructural binary compounds of Sm-Ge and Dy-Ge systems are unlimited. All solid solution forms by mutual substitution of Dy and Sm. The solubility of Sm in $DyGe_3$ is less than 5 at.% Sm. At 873 K we are not confirmed the existence of Dy_3Ge_5 compound, which was presented on the Dy-Ge phase diagram (Fig. 1b)[15], instead, we confirmed the existence of $Dy_{11}Ge_{10}$ phase which earlier was studied by Tharp et al.[18], but is absent in Fig. 1(b).

4.2 Limited Solid Solutions

Limited solid solution from the $SmGe_2$—$DyGe_{1.9}$ section. The SEM/EPMA and XRD phase analysis of alloys (Fig. 3, and Fig. S1) from the isoconcentrate $Sm_{34}Ge_{66}$—$Dy_{34}Ge_{66}$ shows that the $SmGe_2$ (α-$ThSi_2$- type) solve up to 15 at.% Dy and $DyGe_{1.9}$ ($TbGe_2$- type) solve up to 10 at.% Sm. Between these limited solutions, the formation of a new ternary phase of $Dy_2Sm_2Ge_7$ was found (Fig. 3c-e). The lattice parameters for alloys from the homogeneity range of $Sm_{1-x}Dy_xGe_2$ solid solution were determined and refined by powder diffraction data (Table 3 and Fig. 5a). The lattice parameters show an decreasing trend with increasing Dy content and the relative changes of the unit cell volume of $Sm_{1-x}Dy_xGe_2/SmGe_2$ with the increase of Dy content is presented in Fig. 5(a).

According to SEM/EPMA and XRD phase analysis data (Fig. 3b, and Fig. S2) the $DyGe_{1.9}$ ($TbGe_2$- type) solve up to 10 at.% Sm. The lattice parameters for alloys from the homogeneity range of $Dy_{1-x}Sm_xGe_{1.9}$, (x = 0-0.30) solid solution were determined and refined by powder diffraction data are presented in Table 4). The lattice parameters increase with increasing Sm content. The relative changes of the unit cell volume of $Dy_{1-x}Sm_xGe_{1.9}/DyGe_{1.9}$ $Dy_{11-x}Sm_xGe_{10}/Dy_{11}Ge_{10}$ (d) with the increase of Sm content is shown in Fig. 5(b).

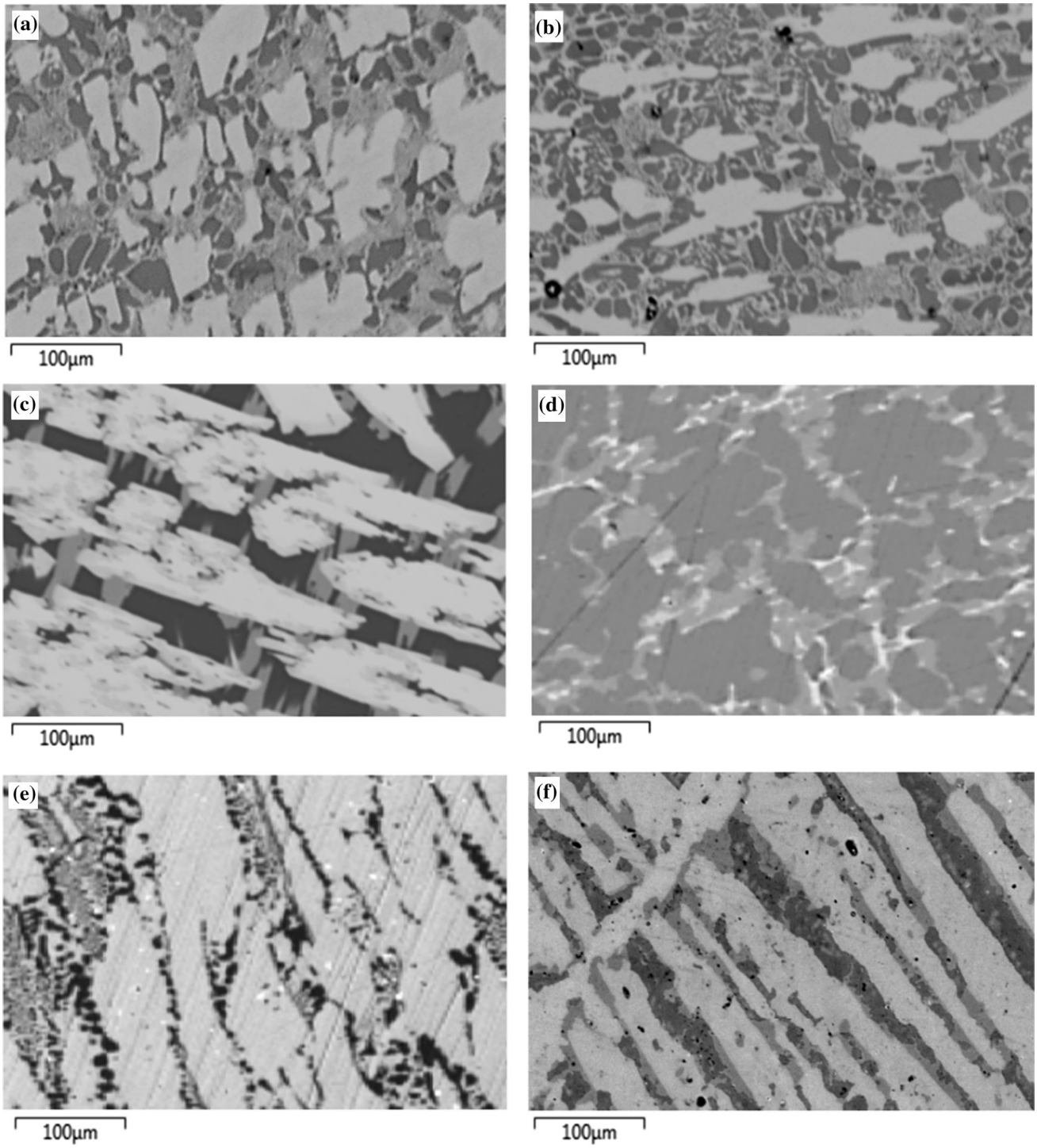

Fig. 4 Micrographs of selected three-phase samples from Dy-Sm-Ge system: (a) $Dy_{21}Sm_{17}Ge_{62}$ (light grey phase—$Dy_{1-x}Sm_xGe_{1.5}$, composition from EPMA $Dy_{22.6(4)}Sm_{17.2(4)}Ge_{60.2(4)}$; grey phase—$Dy_{1-x}Sm_xGe_{1.9}$, $Dy_{24.6(4)}Sm_{9.2(4)}Ge_{66.2(5)}$; dark grey phase—$Dy_2Sm_2Ge_7$, $Dy_{17.4(2)}Sm_{18.1(2)}Ge_{64.5(4)}$; Ge); (b) $Dy_{17}Sm_{21}Ge_{62}$ (light grey phase—$Dy_{1-x}Sm_xGe_{1.5}$, $Dy_{23.1(4)}Sm_{16.8(4)}Ge_{60.1(4)}$; grey phase—$Dy_2Sm_2Ge_7$, $Dy_{17.4(2)}Sm_{18.4(2)}Ge_{64.2(4)}$; Ge); dark grey phase—$Dy_xSm_{1-x}Ge_2$, $Dy_{11.6(4)}Sm_{22.1(4)}Ge_{66.3(5)}$; (c) $Dy_{20}Sm_{26}Ge_{54}$ (light grey phase—$Dy_{1-x}Sm_xGe$, $Dy_{13.0(3)}Sm_{43.6(3)}Ge_{33.4(5)}$; grey phase—$Dy_{1-x}Sm_xGe_{1.5}$, $Dy_{20.2(4)}Sm_{19.6(4)}Ge_{60.2(4)}$; dark grey phase—$Dy_xSm_{1-x}Ge_2$, $Dy_{11.1(4)}Sm_{22.6(4)}Ge_{66.3(5)}$; (d) $Dy_5Sm_{55}Ge_{40}$ (dark grey phase—$Dy_xSm_{1-x}Ge_2$, $Dy_{11.1(4)}Sm_{22.6(4)}Ge_{66.3(5)}$; grey phase—$SmGe_{1.5}$, $Sm_{39.6(3)}Ge_{60.4(4)}$ bright phase—$Dy_{1-x}Sm_xGe$, $Dy_{8.1(3)}Sm_{58.5(3)}Ge_{33.4(5)}$; (e) $Dy_{33}Sm_5Ge_{62}$ (light grey phase—$DyGe_{1.59}$, $Dy_{38.7(3)}Ge_{61.3(4)}$; grey phase—$Dy_{1-x}Sm_xGe_{1.5}$, $Dy_{31.1(4)}Sm_{8.8(4)}Ge_{60.1(4)}$; dark grey phase—$Dy_3Ge_5$, $Dy_{37.6(3)}Ge_{62.4(5)}$; (f) $Dy_{32}Sm_{20}Ge_{48}$ (light grey phase—$Dy_{5-x}Sm_xGe_4$, $Dy_{33.2(2)}Sm_{22.3(2)}Ge_{44.5(3)}$; grey phase—$Dy_{11-x}Sm_xGe_{10}$, $Dy_{43.1(4)}Sm_{9.4(4)}Ge_{47.5(5)}$; dark grey phase—$Dy_{1-x}Sm_xGe$, $Dy_{17.0(3)}Sm_{49.6(3)}Ge_{33.4(5)}$)

Table 3 Composition of alloys and unit cell parameters of $Dy_xSm_{1-x}Ge_2$ (α-$ThSi_2$- type) and $Dy_{11-x}Sm_xGe_{10}$ ($Ho_{11}Ge_{10}$-type) limited solid solutions

Composition of alloys (at.%)			Unit cell dimensions (nm)			V (nm^3)
Sm	Dy	Ge	*a*	*c*	*c/a*	
$Dy_xSm_{1-x}Ge_2$ (α-$ThSi_2$- type)						
34	0	66	0.4171(1)	1.3842(3)	3.3186	0.2408(1)
31	3	66	0.4168(4)	1.3794(3)	3.3095	0.2396(5)
28	6	66	0.4163(2)	1.3780(8)	3.3101	0.2388(3)
25	9	66	0.4159(3)	1.3774(1)	3.3119	0.2383(3)
22	12	66	0.4152(4)	1.3772(1)	3.3170	0.2374(5)
19	15	66	0.4136(2)	1.3770(5)	3.3293	0.2356(2)
18	16	66	0.4136(4)	1.3770(7)	3.3293	0.2356(6)
$Dy_{11-x}Sm_xGe_{10}$ ($Ho_{11}Ge_{10}$- type)						
0	52	48	1.0811(2)	1.6296(4)	1.5074	1.9046(9)
10	42	48	1.08242(9)	1.6334(2)	1.5090	1.9137(3)
15	37	48	1.0824(3)	1.6333(6)	1.5090	1.914(1)

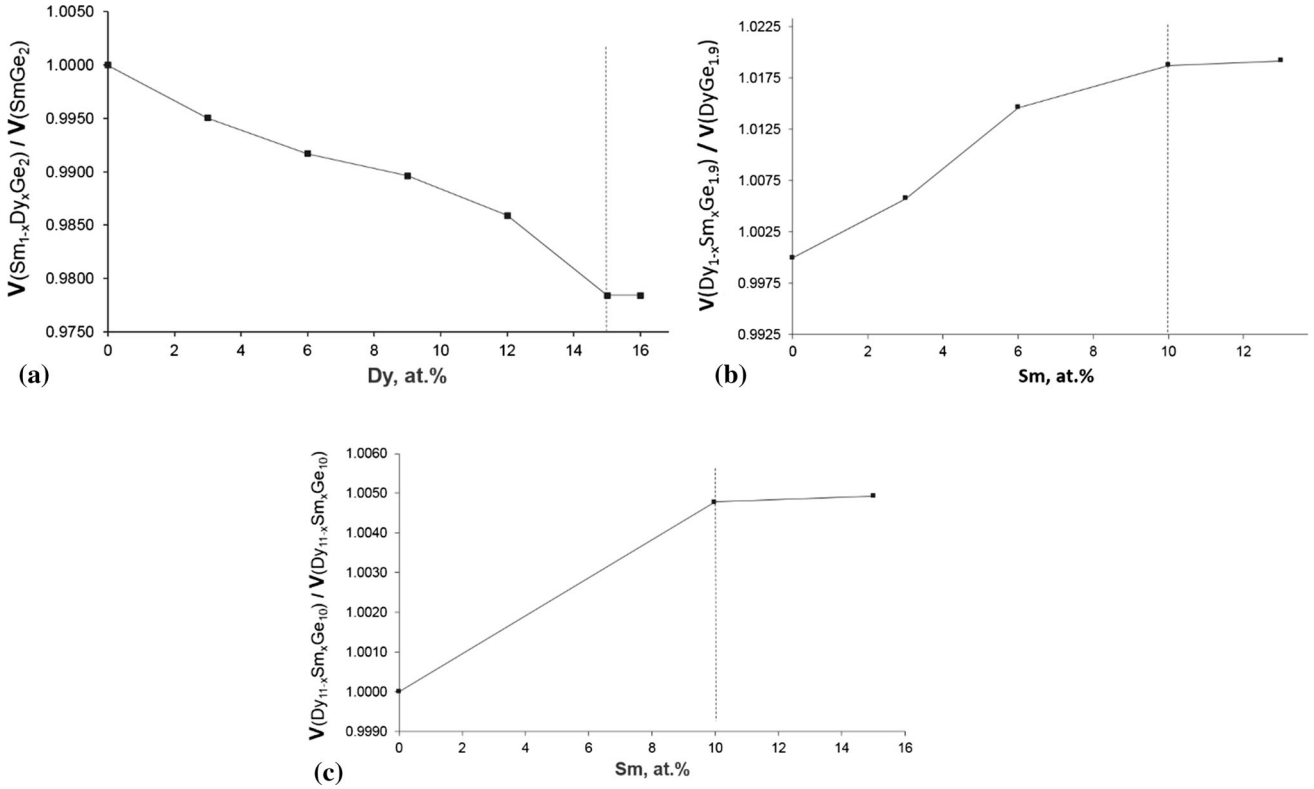

Fig. 5 The relative changes of the unit cell volume of $Sm_{1-x}Dy_xGe_2/SmGe_2$ with the increase of Dy content (a), $Dy_{1-x}Sm_xGe_{1.9}/DyGe_{1.9}$ (b) and $Dy_{11-x}Sm_xGe_{10}/Dy_{11}Ge_{10}$ (c) with the increase of Sm content

$Dy_{11-x}Sm_xGe_{10}$, (x = 0-2.1) limited solid solution. The x-ray diffraction patterns of the studied $Dy_{11-x}Sm_xGe_{10}$, (x = 0 and 2.1) alloys were similar to each other and they corresponded to single phase material with the tetragonal $Ho_{11}Ge_{10}$-type of crystal structure. The alloy with x = 3.1 is no single phase and in addition to the tetragonal phase, contains additional hexagonal $Dy_xSm_{5-x}Ge_3$ and orthorhombic $Dy_xSm_{1-x}Ge$ phases. In Table 3 the appropriate unit cell parameters and calculated unit cell volumes are presented. Careful analysis of the values of the lattice

Table 4 Composition of alloys and unit cell parameters of $Dy_{1-x}Sm_xGe_{1.9}$ ($TbGe_2$- type) limited solid solution

Composition of alloys (at.%)			Unit cell dimensions (nm)			V (nm^3)
Sm	Dy	Ge	*a*	*b*	*c*	
0	34	66	0.4090(3)	2.980(1)	0.3990(2)	0.4863(5)
3	31	66	0.4101(1)	2.9831(6)	0.3998(1)	0.4891(2)
6	26	66	0.4114(1)	2.9943(4)	0.4005(2)	0.4934(3)
10	24	66	0.4120(1)	2.9994(5)	0.4009(1)	0.4954(2)
13	21	66	0.4120(3)	3.0002(6)	0.4009(4)	0.4956(6)

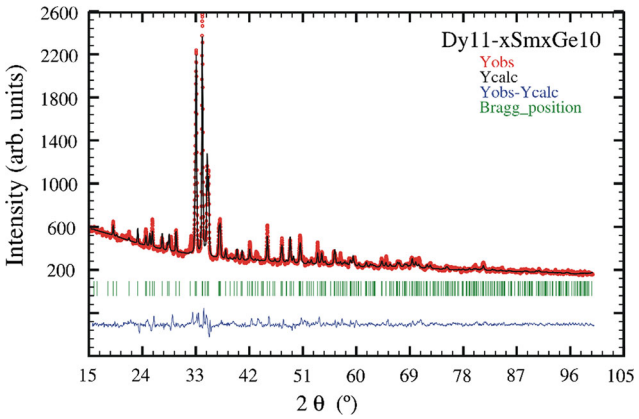

Fig. 6 Observed (circles), calculated (line) and difference (bottom line) x-ray powder diffraction patterns for $Dy_{11-x}Sm_xGe_{10}$ at x = 2.1 (R_p = 5.12, R_{wp} = 6.84, R_{Bragg} = 10.01, R_f = 9.35). Vertical bars indicate the Bragg positions

parameters and the unit cell volumes indicates insignificant increase of these parameters with partial substitution of Dy by Sm atoms up to 10 at.% (Fig. 5c). Rietveld refinement of the crystal structure of this solid solution for the alloy with x = 2.1 (Fig. 6) showed that the substitution of Dy by Sm occurs in two crystallographic positions *8h* and *4e*. At the final, all parameters were refined up to R_B = 8.27, R_F = 6.93, R_p = 5.12, R_{wp} = 6.84 and χ^2 = 1.47.

4.3 Continuous Solid Solutions

Three series $Dy_{1-x}Sm_xGe$, $Dy_{5-x}Sm_xGe_3$ and $Dy_{5-x}Sm_xGe_4$ of continuous solid solutions at the 873 K in the Dy-Sm-Ge system are observed. The SEM micrographs of selected samples from homogeneity regions of continuous solid solutions show their almost single phase state (Fig. S3).

$Dy_{1-x}Sm_xGe$, (x = 0-1) continuous solid solution. Both equiatomic binary DyGe and SmGe compounds crystallises in a orthorhombic CrB—type in which the *4c* crystallographic site occupy atoms of rare earth metals. Between these binary compound four ternary alloys were prepared and studied by SEM, EPMA (Fig. S3a-c) and XRD (Fig. S4) method of analysis. Almost linear changes in the unit cell parameters and volume are observed in fully concentration range of this solid solution (Table 5) The relative changes of the unit cell volume of $Dy_{1-x}Sm_xGe$/DyGe with the increase of Sm content is presented in Fig. 7(a).

$Dy_{5-x}Sm_xGe_3$, (x = 0-5) continuous solid solution. The $Dy_{5-x}Sm_xGe_3$ (x = 0-5) continuous solid solution was detected by SEM, EPMA (Fig. 8d-f) and XRD (Fig. S5) methods on the Dy_5Ge_3—Sm_5Ge_3 section. All samples consist hexagonal phase with Mn_5Si_3 structure type. This solid solution is formed by mutual substitution of rare earth metals (Sm and Dy). The lattice parameters for alloys from the homogeneity range of this solid solution were determined and refined by powder diffraction data (Table 6). The relative changes of the unit cell volume of $Dy_{5-x}Sm_xGe_3$/Dy_5Ge_3 obtained in this work show a tendency to increase cell volume with increasing Sm content (Fig. 7b).

$Dy_{5-x}Sm_xGe_4$, (x = 0-5) continuous solid solution. Six alloys from the Dy_5Ge_4—Sm_5Ge_4 section were prepared and analysed by SEM/EPMA (Fig. S3j-i) and XRD (Fig. 7c) methods. Both binary phases crystallises in orthorhombic Sm_5Ge_4-type. The x-ray powder diffraction patterns obtained for all the investigated alloy samples were completely indexed on the basis of the Sm_5Ge_4-type structure by the assuming a statistical distribution of the Dy and Sm atoms on the both *8d* and *4c* sites. The Rietveld analysis (Fig. 8) performed for the alloy of the $Dy_{20}Sm_{35.5}Ge_{44.5}$ composition has shown that the distribution of its constituent atoms of rare earth metals in all sites are an statistical mixed. The structural parameters were refined up to R_B = 6.43, R_F = 5.92, R_p = 2.34, R_{wp} = 3.07 and χ^2 = 0.33. The lattice parameters for alloys from the homogeneity range of this solid solution are presented in Table 5 and Fig. 7(c) presents the relative changes of the unit cell volume of $Dy_{5-x}Sm_xGe_4$/Dy_5Ge_4 with the increase of Sm content.

Table 5 Composition of alloys and unit cell parameters of $Dy_{1-x}Sm_xGe$ (CrB-type) and $Dy_{5-x}Sm_xGe_4$ (Sm_5Ge_4-type) continuous solid solutions

Composition of alloys (at.%)			Unit cell dimensions (nm)			V (nm^3)
Sm	Dy	Ge	*a*	*b*	*c*	
$Dy_{1-x}Sm_xGe$ (CrB-type)						
0	50	50	0.42719(8)	1.0678(3)	0.39309(6)	0.17931(7)
10	40	50	0.4288(3)	1.0692(6)	0.3935(3)	0.1804(2)
20	30	50	0.4309(2)	1.0739(5)	0.3961(3)	0.1833(2)
30	20	50	0.4338(5)	1.0774(5)	0.3972(4)	0.1856(3)
40	10	50	0.4353(7)	1.0817(8)	0.3982(6)	0.1875(4)
50	0	50	0.4387(1)	1.0891(6)	0.3993(1)	0.1908(1)
$Dy_{5-x}Sm_xGe_4$ (Sm_5Ge_4-type)						
0	55.5	44.5	0.7580(2)	1.4592(2)	0.7603(2)	0.8410(3)
15.5	40.0	44.5	0.7619(1)	1.4752(3)	0.7659(3)	0.8608(4)
35.5	20.0	44.5	0.76851(3)	1.4819(2)	0.7706(1)	0.8776(1)
45.5	10.0	44.5	0.7719(2)	1.4889(4)	0.7760(2)	0.8918(4)
55.5	0	44.5	0.7751(1)	1.4950(3)	0.7825(1)	0.9067(3)

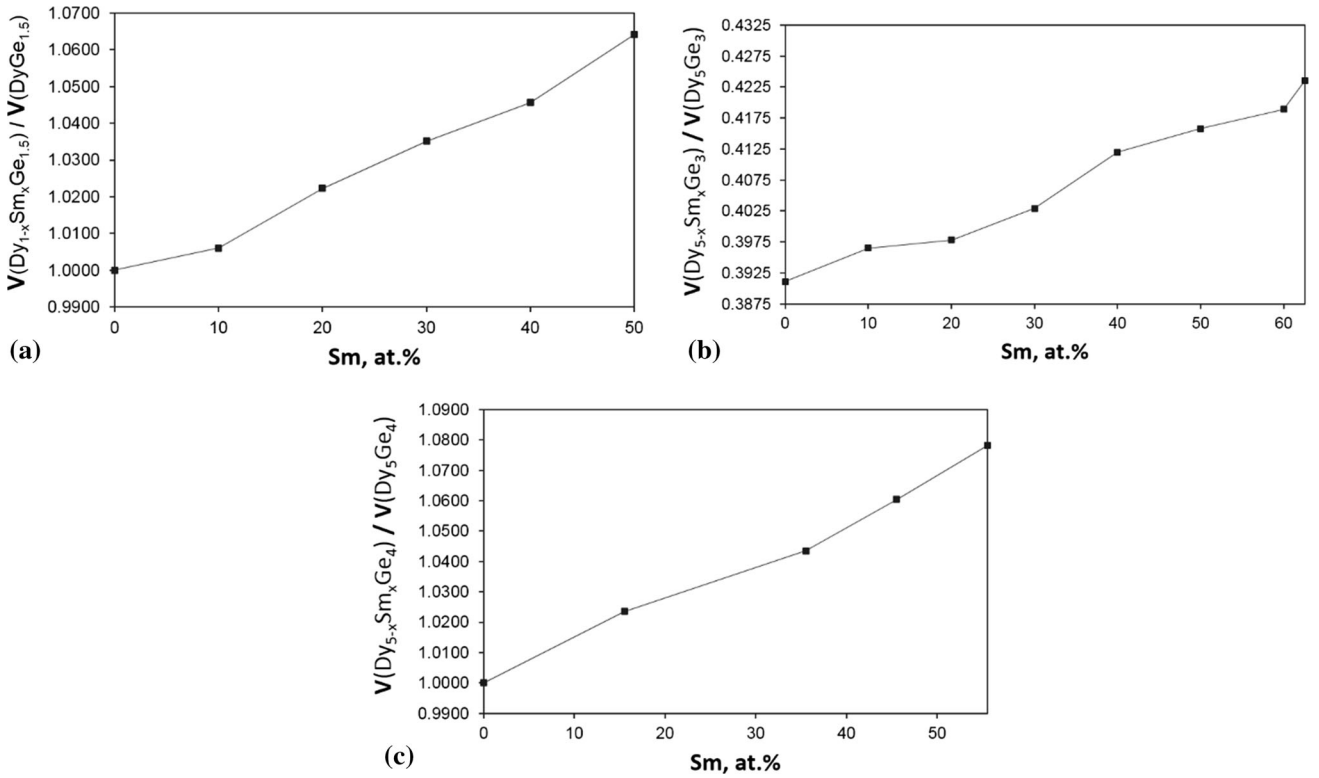

Fig. 7 The relative changes of the unit cell volume of $Dy_{1-x}Sm_xGe/DyGe$ (a), $Dy_{5-x}Sm_xGe_3/Dy_5Ge_3$ (b), $Dy_{5-x}Sm_xGe_4/Dy_5Ge_4$ (c) with the increase of Sm content

4.4 Ternary Compounds

4.4.1 $Dy_2Sm_2Ge_7$ Ternary Compound

During a study of alloys from the $Sm_{34}Ge_{66}$—$Dy_{34}Ge_{66}$ concentration section the formation of a new ternary phase of $Dy_2Sm_2Ge_7$ was found. The powder diffraction pattern indicated that the $Dy_{17}Sm_{14}Ge_{66}$ alloy consists as main phase of the $Dy_2Sm_2Ge_7$ and small amounts of Ge (Fig. 9a). The irregular form single crystal was extracted from this alloy after its defragmentation (Fig. 9b) and diffraction pattern is presented in Fig. 9(c). The crystal

structure of $Dy_2Sm_2Ge_7$ was investigated by single crystal experiments and was successfully solved by direct methods using SHELX-97 package programs. This compound may be viewed as the ordered superstructure to Nd_4Ge_7-type.[14] The orthorhombic unit cell with $C222_1$ space group of this intermetallic compound contains 44 atoms occupying 7 different Wyckoff sites. In the Nd_4Ge_7-type the all neodymium atoms occupy the *4a*, *4b* and *8c* sites, instead, in the $Dy_2Sm_2Ge_7$ ternary phase, the first two sites occupy the atoms of dysprosium, and the third site is occupied by the atoms of samarium. This distribution of atoms gives the nominal composition of $Sm_{18.2}Dy_{18.2}Ge_{63.6}$, which is very consistent with the composition $Sm_{18.2(2)}Dy_{17,7(2)}Ge_{64,1(3)}$ received from EPMA data. The crystal data and refined atomic parameters for $Dy_2Sm_2Ge_7$ are listed in Tables 7 and 8 respectively. The structural parameters from single crystal was confirmed by Rietveld refinements of powder data (R_p = 4.99, R_{wp} = 6.36, R_B = 8.11, R_F = 9.73 and χ^2 = 1.15). The projection of the unit cell and coordination polyhedra of the atoms is shown in Fig. 10. The distorted equatorial four-capped trigonal prisms [RGe_{10}] are typical for all rare-earth atoms. The germanium atoms are enclosed in to tricapped trigonal prisms. The germanium atoms form 3D network (Fig. 11a) and atoms of rare-earth metals form filled and empty trigonal prisms which a linked by lateral faces (Fig. 11b). The electronic structure calculations by TB-LMTO-ASA confirm the existence of 3D network and the isosurfaces of electron localization function (ELF) around the Ge atoms at the 0.70 level is presented in Fig. 12(a).

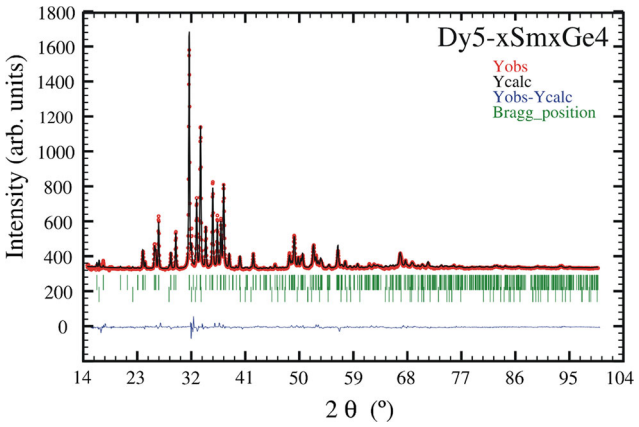

Fig. 8 Observed (circles), calculated (line) and difference (bottom line) x-ray powder diffraction patterns for $Dy_{5-x}Sm_xGe_4$ at x=3.2 (R_p = 3.62, R_{wp} = 5.30, R_{Bragg} = 7.31, R_f = 6.74). Vertical bars indicate the Bragg positions

The distribution of electron localization function around Ge atoms and crystal chemical analysis suggest that 3D network from germanium atoms form negatively charged $n[Ge_7]^{4m-}$ polyanions, which are compensated by positively charged $2nDy^{m+}$ and $2nSm^{m+}$ polycations. It should be noted, that for intermetallics there are known examples of compounds with polyanions, here are some of the previously investigated: LiGe, ($n[Ge_6]^{4-}$ polyanion),[40] Li_4Ge_2B ($n[B_3Ge_6]^{m-}$),[41] $Li_9Al_4Sn_5$ ($n[Al_4Sn_5]^{m-}$),[42] $TmNi_{1-x}Li_xSn_2$ ($n[Sn]^{m-}$)[43] and $La_4Mg_5Ge_6$ ($n[Mg_5Ge_6]^{\delta-}$).[44]

The description of chemical bonding used by us to some extent was based on the Zintl-Klemm concept according to which structure consists of a polyanion with cations located between the anionic lattice. In the typical Zintl phases the anion-cation interaction prevails, and they have low conductivity, or semiconductivity. This causes an insignificant density of states or a pseudo-gap at the Fermi level. The $Dy_2Sm_2Ge_7$ structure, like other similar phases well-known from literature, has a predominant metallic bonding, and cation-anion interaction is an additional interaction based on partial charges.

The total and partial density of states (DOS) for the $Dy_2Sm_2Ge_7$ is shown in Fig. 12(b). The higher density of

Table 6 Composition of alloys and unit cell parameters of $Dy_{5-x}Sm_xGe_3$ (Mn_5Si_3-type) continuous solid solution

Composition of alloys (at.%)			Unit cell dimensions, nm			V, nm^3
Sm	Dy	Ge	*a*	*c*	*c/a*	
0	62.5	37.5	0.8442(2)	0.6337(4)	0.7507	0.3911(3)
10.0	52.5	37.5	0.8482(2)	0.6364(3)	0.7503	0.3965(3)
20.0	42.5	37.5	0.8489(2)	0.6375(3)	0.7510	0.3978(3)
30.0	32.5	37.5	0.8525(3)	0.6401(4)	0.7509	0.4029(4)
40.0	22.5	37.5	0.8583(7)	0.6457(9)	0.7523	0.4120(9)
50.0	12.5	37.5	0.8618(2)	0.6464(2)	0.7501	0.4158(2)
60.0	2.5	37.5	0.8654(3)	0.6459(3)	0.7464	0.4189(4)
62.5	0	37.5	0.8661(2)	0.6519(2)	0.7527	0.4235(2)

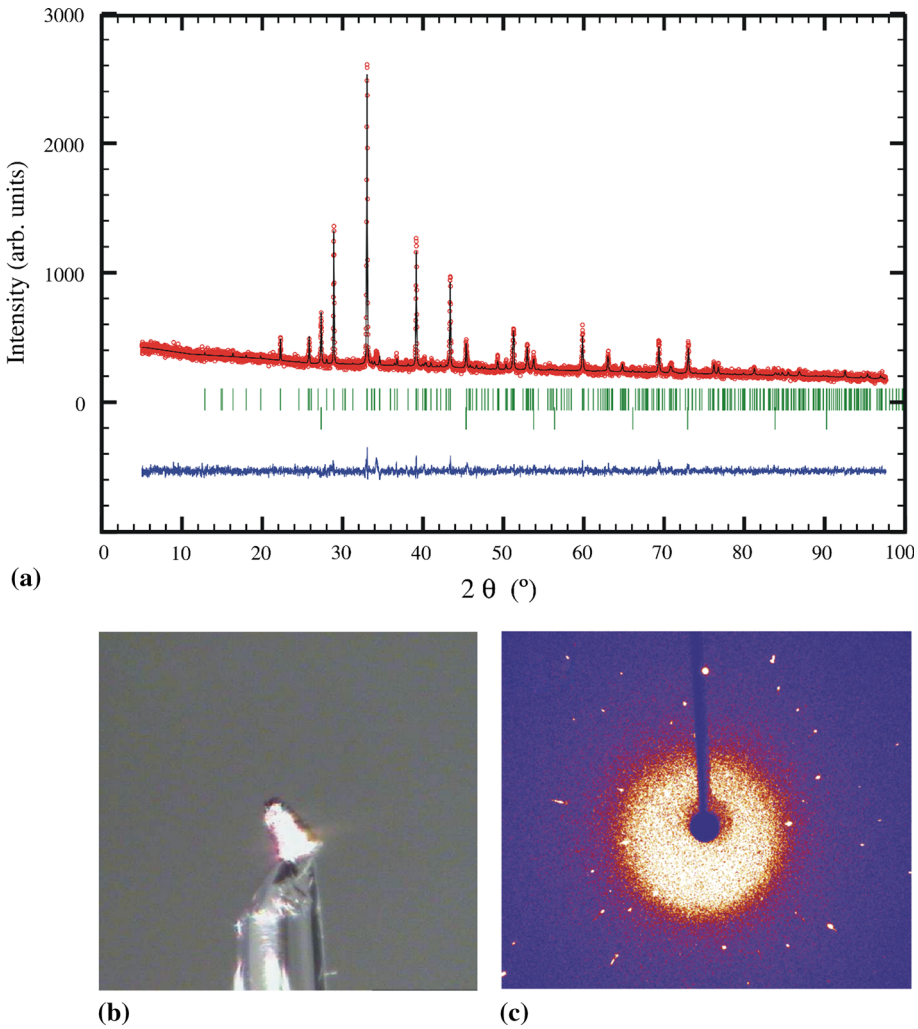

Fig. 9 Observed (circles), calculated (line) and difference (bottom line) x-ray powder diffraction patterns for $Dy_2Sm_2Ge_7$ (R_p = 4.99, R_{wp} = 6.36, R_B = 8.11, R_F = 9.73) (a). Image of single crystal (b) and diffraction pattern of $Dy_2Sm_2Ge_7$ single crystal (c)

electronic states at the Fermi level confirm the metallic behaviour. The feature of this structure is a very intense peaks from the overlapping of the *f* orbitals of Dy and Sm with *p* orbital of Ge in the valence band nearly Fermi level.

4.4.2 $Dy_{1-x}Sm_xGe_{1.5}$ (x = 0.15-0.50) Ternary Phase

The samples of the compositions $Dy_{40}Ge_{60}$, $Dy_{35}Sm_5Ge_{60}$, $Dy_{30}Sm_{10}Ge_{60}$, $Dy_{20}Sm_{20}Ge_{60}$ and $Dy_{10}Sm_{30}Ge_{60}$ were prepared and investigated by the XRD powder method (Fig. S6a). The extent of homogeneity region of $Dy_{1-x}Sm_xGe_{1.5}$, (x = 0.15-0.50) ternary phase was determined by the change in lattice parameters. The change in lattice parameters with varying concentrations of Sm are presented in Table 9. From the data of Table 9 it is obvious that replacement of Dy atoms by Sm atoms increases the unit cell volume of $Dy_{1-x}Sm_xGe_{1.5}$.

Rietveld matrix full-profile structure refinements confirm well the powder patterns calculated on the basis of defected AlB_2 structure model (Fig. S6b). The *1a* site fully occupied by statistical mixture of Dy and Sm atoms and the germanium atoms partially occupy the *2d* site. For the $Dy_{1-x}Sm_xGe_{1.5}$ (x = 0.25) ternary phase after last cycle refinement the residual factors are: Rp = 6.57, Rwp = 8.93, R_B = 8.37, R_f = 8.87, and χ^2 = 1.54.

The $Dy_{1-x}Sm_xGe_{1.5}$ is a ternary compound with wide homogeneity of region, and can be interpreted as a residue of a high-temperature solid solution based on high temperature phase γ-$DyGe_{1.5}$. It is known that germanium-rich phases exhibit structural instability and, depending on the

Table 7 Crystal data and structure refinement

Empirical formula	$Dy_2Sm_2Ge_7$
Formula weight	1133.83
Temperature	T = 293 K
Wavelength	MoKα, 0.71073 nm
Crystal system, space group	orthrhombic, $C222_1$ (20)
Unit cell dimensions	a = 0.59425(12) nm
	b = 1.3823(3) nm
	c = 1.1801(2) nm
Volume	0.9694(3) nm^3
Calculated density	7.769 g/cm^3
Absorption coefficient	48.39 mm^{-1}
F(000)	1920
Theta range for data collection	θ_{max} = 27.5°, θ_{min} = 3.0°
Index ranges	− 7 < =h < =7,
	− 17 < =k < =17,
	− 15 < =l < =15
Reflections collected/unique	4404/1110
Refinement method	Refinement on F^2
	Least-squares matrix: full
Data/parameters	1110/52
Goodness of fit on F^2	1.13
$R[F^2 > 2\ \sigma(F^2)]$	0.028
$wR(F^2)$	0.088
Largest diff. peak and hole	1.58 and − 2.16 e $Å^{-3}$

conditions and methods of synthesis, the purity of metals, some phases may not form, and some, on the contrary, can stabilize (the formation of metastable phases). Also, the addition of a third component to binary germanides can lead to the stabilization of structures that are typical for metastable phases (as in the case of Sm_4Ge_7 and $Dy_2Sm_2Ge_7$), or also stabilization of structures that are typical for high-temperature phases (as in the case of $DyGe_{1.5}$ and $Dy_{1-x}Sm_xGe_{1.5}$). Similar cases are known in the literature, for example, in system Sm-Ni-Ge[45] and Sm-Rh-Ge,[46] the ternary phases $SmNi_{0.5}Ge_{1.5}$ and $SmRh_{0.6}Ge_{1.4}$ with the AlB_2 structure type also formed at 600°C, although high temperature phase $SmGe_{1.5}$ (AlB_2-type structure) exist above 1085°C). It should be noted that the formation of superstructures to binary phases, as well as the decreasing of the temperature of formation of high-temperature phases at the addition of the third component, were found in other systems which do not contain germanium, such as La-Ni-Zn,[47] Mn-Al-Li[48] etc.

5 Summary

The isothermal section of phase diagram of the Dy-Sm-Ge system was studied in the full concentration range by means of x-ray phase and structural analyses, microstructural analysis and energy dispersive x-ray spectroscopy. Phase relations of this system were determined at 873 K by characterizing of 56 alloys. The features of this system are

Table 8 Fractional atomic coordinates and thermal displacement parameters ($Å^2$) for $Dy_2Sm_2Ge_7$

Atoms	Site	*x/a*	*y/a*	*z/a*	U_{iso}*/U_{eq}	Occ.
Sm1	*8(c)*	0.2527 (1)	0.25203 (4)	0.37847 (5)	0.0123 (2)	1.0
Dy1	*4(a)*	0.0021 (1)	0.0000	0.0000	0.0102 (2)	1.0
Dy2	*4(b)*	0.0000	0.49901 (5)	0.2500	0.0169 (2)	1.0
Ge1	*8(c)*	0.2521 (2)	0.1682 (1)	0.1446 (1)	0.0189 (3)	1.0
Ge2	*8(c)*	0.3143 (2)	0.3582 (1)	0.1549 (2)	0.0246 (4)	1.0
Ge3	*8(c)*	0.5023 (2)	0.0894 (1)	0.0018 (1)	0.0182 (3)	1.0
Ge4	*4(b)*	0.0000	0.0591 (1)	0.2500	0.0192 (4)	1.0

	U^{11}	U^{22}	U^{33}	U^{12}	U^{13}	U^{23}
Sm1	0.0123 (3)	0.0120 (4)	0.0125 (3)	0.0001 (2)	− 0.0006 (3)	0.0002 (2)
Dy1	0.0101 (3)	0.0105 (4)	0.0100 (4)	0.000	0.000	0.0004 (3)
Dy2	0.0166 (4)	0.0168 (4)	0.0172 (4)	0.000	− 0.0004 (4)	0.000
Ge1	0.0178 (6)	0.0189 (6)	0.0200 (8)	− 0.0001 (5)	0.0004 (7)	0.0001 (6)
Ge2	0.0222 (6)	0.0217 (6)	0.030 (1)	0.0000 (5)	− 0.0010 (7)	− 0.0004 (7)
Ge3	0.0186 (6)	0.0191 (6)	0.0170 (7)	0.0000 (5)	− 0.0008 (7)	0.0003 (6)
Ge4	0.0207 (9)	0.0188 (9)	0.018 (1)	0.000	− 0.001 (1)	0.000

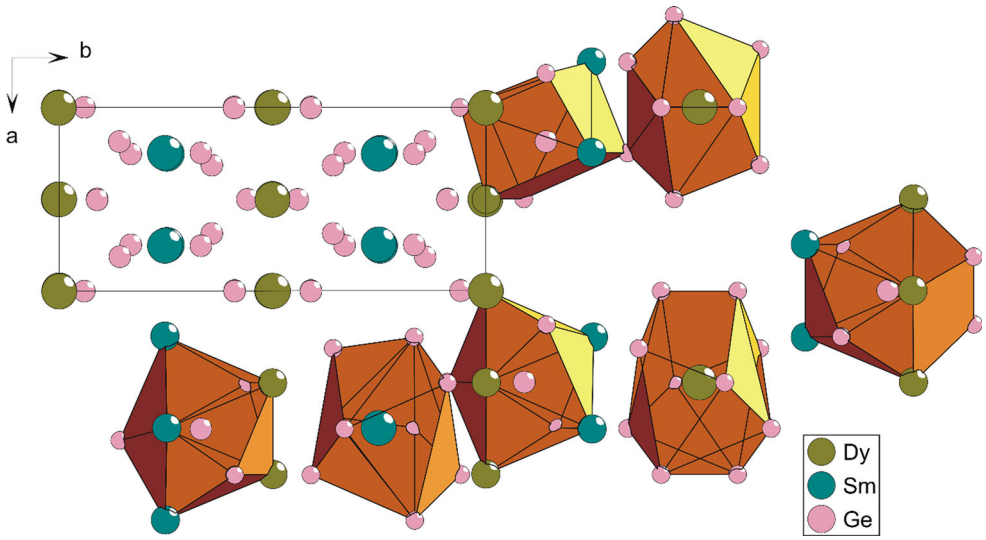

Fig. 10 Unit cell and coordination polyhedra of atoms in the $Dy_2Sm_2Ge_7$

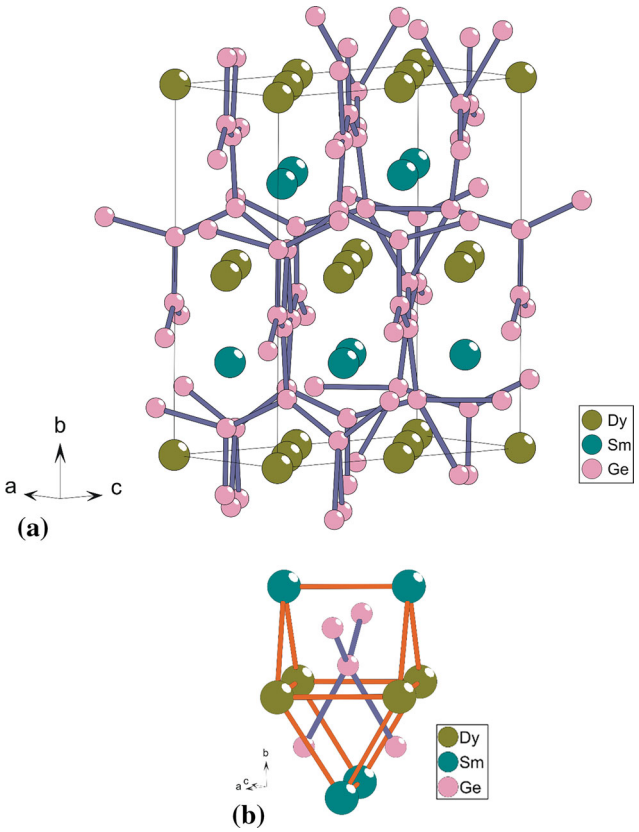

Fig. 11 The germanium atomic 3D network (a) and kind of linking of the filled and empty trigonal prisms (b)

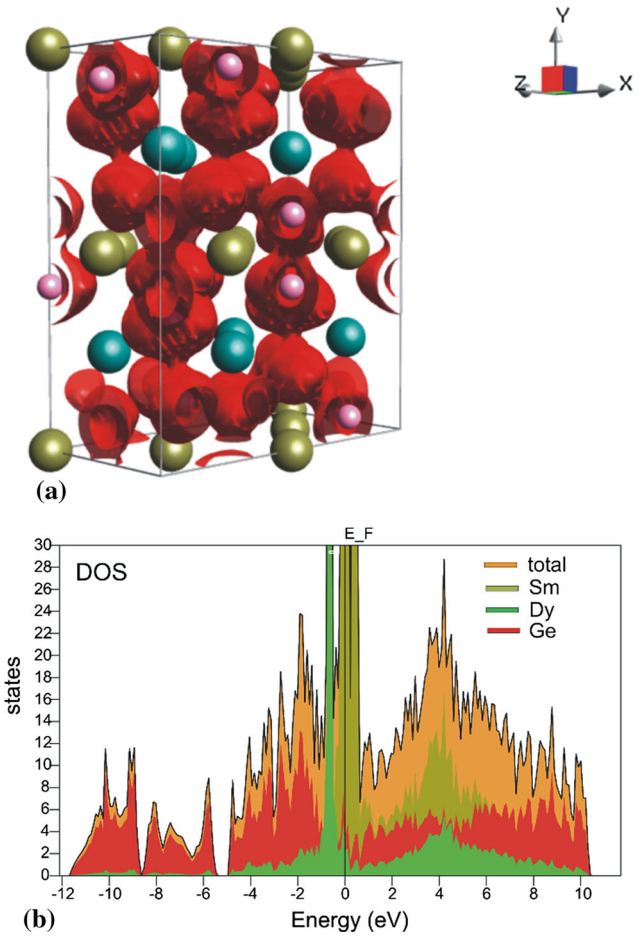

Fig. 12 The isosurfaces of the ELF around the atoms (a) and total and partial DOS (b) in the $Dy_2Sm_2Ge_7$ structure

the formation of continuous solid solutions: $Dy_{1-x}Sm_xGe$ (x = 0-1), $Dy_{5-x}Sm_xGe_3$ (x = 0-5) and $Dy_{5-x}Sm_xGe_4$, (x = 0-5), and limited solid solutions: $Dy_{1-x}Sm_xGe_{1.9}$, (x = 0-0.30), $Dy_xSm_{1-x}Ge_2$ (x = 0-0.45) and $Dy_{11-x}Sm_xGe_{10}$, (x = 0-2.1). All solid solutions are formed by the mutual substitution of atoms of rare earth metals.

Two ternary $Dy_{1-x}Sm_xGe_{1.5}$ (x = 0.15-0.50) and $Sm_2Dy_2Ge_7$ compounds were found. The crystal structure of $Sm_2Dy_2Ge_7$ was investigated by means of x-ray single crystal diffraction: Pearson symbol *oS*44, space group

Table 9 Composition of alloys and unit cell parameters of $Dy_{1-x}Sm_xGe_{1.5}$ (AlB_2-type) ternary phase

Composition of alloys (at.%)			Unit cell dimensions (nm)			V (nm^3)
Sm	Dy	Ge	*a*	*c*	*c/a*	
5	35	60	0.39314(6)	0.4131(1)	1.0508	0.05529(2)
10	30	60	0.39395(4)	0.41696(5)	1.0584	0.05604(1)
20	20	60	0.39703(5)	0.41967(7)	1.0570	0.05729(2)
30	10	60	0.3974(7)	0.4197(1)	1.0561	0.0574(2)

$C222_1$, a = 0.5942(1), b = 1.3823(4), c = 1.1801(3) nm, V = 0.9694 nm^3. This compound is ordered superstructure to Nd_4Ge_7-type. The electronic structure was calculated by the tight-binding linear muffin-tin orbital atomic spheres approximation method. The electron localization function is higher around the Ge atoms, which form an $n[Ge_7]^{4m-}$ polyanion.

Acknowledgments Financial support from the National Science Centre, Poland (No 2017/25/B/ST8/02179) is gratefully acknowledged.

References

1. W.E. Wallace, *Rare Earth Intermetallics*, Academic Press, New York and London, 1973
2. *Handbook on the Physics and Chemistry of Rare Earths*. Edited by J.-C. G. Bünzli and V. K. Pecharsky, 2016, 50, p 2–427
3. Z. Shpyrka and L. Drab, The Investigation of the Section DyGe2-RGe2, Where R-Y, Gd, Tb, Ho, Er, Tm and Lu at 600 C, Visnyk Lviv University, *Ser. Khim.*, 2008, **49**, p 98-102
4. V. Vorotnyak, Z. Shpyrka, V. Pavlyuk and R. Serkiz, The Crystal Structure of the $Dy_{0.67}Tm_{0.33}Ge_{1.85}$ Compound, *Visnyk Lviv University, Ser. Khim*., 2012, **53**, p 66–71
5. Z. Shpyrka., O. Bodak and P. Starodub, The Crystal Structure of the $Dy_{0.5}Ho_{0.5}Ge_{1.75}$ Compound, *Visnyk Lviv University, Ser. Khim.,* 2002, **41**, p 80–82
6. Z. Shpyrka, V.Pavlyuk, D. Berezyuk and P. Starodub, The crystal structure of the $Dy_{0.6}Lu_{0.4}Ge_2$ compound, *Coll. Abstr. XII conf. "Lviv Chemical Readings-2009"*, *Lviv*, 2009, p H58
7. Z. M. Shpyrka, O. I. Bodak, I. R. Mokra and V. K. Pecharskij, Crystal structure of the $Sm_{0.625}Lu_{0.375}Ge_{1.85}$, *Coll. Abstr. VI Intern. Conf. on Crystal Chemistry of Intermetallic Compounds, Lviv,* 1995, p 94
8. A.B. Gokhale and G.J. Abbaschian, The Ge-Sm (Germanium–Samarium) System, *Bull Alloy Phase Diagr*, 1988, **9**, p 578-581
9. V.N. Eremenko, V.G. Batalin, and YuI, Buyanov, Phase Diagrams of Samarium–Germanium, *Dop. Akad. Nauk Ukr. RSR B.*, 1977, **5**, p 413-416
10. G. Venturini, Y. Ijjaali, and B. Malaman, Vacancy Ordering in AlB_2—type RGe_{2-x} Compounds (R = Y, Nd, Sm, Gd-Lu), *J. Alloys Compd.*, 1999, **284**, p 262-269
11. P.H. Tobash, D. Lins, S. Bobev, N. Hur, J.D. Thompson, and J.L. Sarrao, Vacancy Ordering in $SmGe_{2-x}$ and $GdGe_{2-x}$ (x = 0.33): Structure and Properties of Two Sm_3Ge_5 Polymorphs and of Gd_3Ge_5, *Inorg. Chem.*, 2006, **45**(18), p 7286-7294
12. I. Mayer and Y. Eshdat, MSi_xGe_{2-x} Ternary Phases of the Rare Earth Metals, *Inorg. Chem.*, 1968, **7**, p 1904-1908
13. G. Venturini, I. Ijjaali, and B. Malaman, New Ordered $ThSi_2$-type Derivatives in the Light Rare Earths Germanides. Crystal Structure of Nd_4Ge_7, *J. Alloys Compd.*, 1999, **289**, p 168-177
14. J. Zhang, P.H. Tobash, W.D. Pryz, D.J. Buttey, N. Hur, J.D. Thompson, J.L. Sarrao, and S. Bobev, Synthesis, Structural Characterization, and Physical Properties of the Early Rare-Earth Metal Digermanides $REGe_{2-x}$ ($x \approx 1/4$) [RE = La-Nd, Sm]. A Case Study of Commensurately and Incommensurately Modulated Structures, *Inorg. Chem.*, 2013, **52**(2), p 953-964
15. K. Meier, C. Koz, A. Kerkau, and U. Schwarz, Crystal Structure of Samarium Pentagermanide, $SmGe_5$, *New Cryst. Struct.*, 2009, **224**(3), p 349-350
16. K. Meier, A. Wosylus, R.H. Cardoso Gil, U. Burkhardt, C. Curfs, M. Hanfland, Y. Grin, and U. Schwarz, New Rare-Earth Metal Germanides RE_2Ge_9 (RE= Nd, Sm) by Thermal Decomposition of High-Pressure Phases $REGe_5$, *Z. Anorg. Allg. Chem.*, 2012, **638**, p 1446-1451
17. V.N. Eremenko, V.G. Batalin, YuI, Buyanov, and I.M. Obushenko, The Dy-Ge Phase Diagram, *Dop. Akad. Nauk Ukr. RSR B*, 1977, **6**, p 516-521
18. I. Mayer and I. Shidlovsky, M_5X_3-Type Rare Earth Silicides and Germanides and Their Ternary Phases with Carbon, *Inorg. Chem.*, 1969, **8**(6), p 1240-1243
19. G.S. Smith, A.G. Tharp, and Q. Johnson, Rare Earth-Germanium and-Silicon Compounds at 5:4 and 5:3 Compositions, *Acta Cryst.*, 1967, **22**, p 940-943
20. A.G. Tharp, G.S. Smith, and Q. Johnson, Structures of the Rare-Earth Germanides at or Near Equiatomic Proportions, *Acta Cryst.*, 1966, **20**, p 583-585
21. K. Sekizawa, Magnetic and Crystallographic Studies on Rare Earth Germanides, *J. Phys. Soc. Jpn.*, 1966, **21**, p 1137-1142
22. E.I. Gladyshevskii, Crystal Structure of the Digermanide of Rare Earth Elements, *J. Struct. Chem.*, 1964, **5**, p 523-529
23. G. Venturini, I. Ijjaali, and B. Malaman, RGe_{2-x} Compounds (R= Y, Gd-Ho) with New Ordered $ThSi_2$-Defect Structures, *J. Alloys Compd.*, 1999, **285**, p 194-203
24. I.R. Mokra, V.K. Pecharskii, Z.M. Shpyrka, O.I. Bodak, V.K. Belsky and I.E. Patz, Crystal Structure of the $DyGe_{1.85}$, *Dopov. Akad. Nauk Ukr. RSR Ser. B*, 1989, p 3–45.
25. P. Schobinger Papamantellos, D.B. De Mooij, and K.H.J. Buschow, Crystallographic and Magnetic Structure of Dy_3Ge_5 and $DyGe_{1.9}$, *J. Less-Common Met.*, 1990, **163**, p 319-330
26. P. Schobinger Papamantellos, D.B. De Mooij, and K.H.J. Buschow, Crystal Structure of the Compound $DyGe_3$, *J. Alloys Compd.*, 1992, **183**, p 181-186
27. P.H. Tobash, S. Bobev, J.D. Thompson, and J.L. Sarrao, Polymorphism in Binary Rare-Earth Metal Germanides. Synthesis, Structure and Properties of the New Hexagonal forms of Tb_3Ge_5 and Dy_3Ge_5, *J. Alloys Compd.*, 2009, **488**, p 533-537
28. O. Oleksyn, P. Schobinger Papamantellos, C. Ritter, C.H. De Groot, and K.H.J. Buschow, Antiferromagnetic Ordering in the Novel Dy_3Ge_4 and $DyGe_{1.3}$ Compounds Studied by Neutron Diffraction and Magnetic Measurements, *J. Alloys Compd.*, 1997, **262**(263), p 492-497
29. A.V. Tsvyashchenko, A.V. Spasskiy, A.I. Velichkov, A.V. Salamatin, L.N. Fomicheva, D.A. Salamatin, G.K. Ryasny, A.V. Nikolaev, M. Budzynski, and R.A. Sadykov, ^{111}Cd-TDPAC

Study of Pressure Effect on the Valence of Yb in the $YbGe_{2.85}$ Cubic Phase, *J. Alloys Compd.*, 2013, **552**, p 190-194
30. Desk Handbook: Phase Diagrams for Binary Alloys, Ed. by H. Okamoto, Materials Park (OH), American Society for Metals, 2000, p 828
31. J. Rodriguez-Carvajal, Recent Developments in the Program FullProf, in Commission on Powder Diffraction (IUCr), *Newsletter*, 2001, **26**, p 12-19
32. CrysAlis PRO. UK Ltd, Yarnton, Oxfordshire, England, Agilent Technologies, 2011
33. G.M. Sheldrick, *SHELXS, Program for the Solution of Crystal Structures*, University of Goettingen, Goettingen, 1997
34. G.M. Sheldrick, *SHELXL-97, Program for Crystal Structure Refinement*, University of Goettingen, Goettingen, 1997
35. O.K. Andersen, Linear Methods in Band Theory, *Phys. Rev. B*, 1975, **12**, p 3060-3083
36. O.K. Andersen and O. Jepsen, Explicit, First-Principles Tight-Binding Theory, *Phys. Rev. Lett.*, 1984, **53**, p 2571-2574
37. O.K. Andersen, Z. Pawlowska, and O. Jepsen, Illustration of the Linear-Muffin-Tin-Orbital Tight-Binding Representation: Compact Orbitals and Charge Density in Si, *Phys. Rev. B*, 1986, **34**, p 5253-5270
38. U. von Barth and L. Hedin, A Local Exchange-Correlation Potential for the Spin Polarized Case, *J. Phys. C Solid State*, 1972, **5**, p 1629-1642
39. Eck, B. wxDragon 1.6.6, Aachen, 1994–2010 [cited 2013 Apr 7]; Available from: http://www.ssc.rwth-aachen.de.
40. V. Pavlyuk, W. Ciesielski, D. Kulawik, W. Prochwicz, and B. Rozdzynska-Kiełbik, Li-Ge-H System: Hydrogenation and Structural Properties of $LiGeH_x$ ($0 < x < 0.25$) Phase, *Solid State Sciences*, 2016, **61**, p 24-31
41. V. Pavlyuk, W. Ciesielski, B. Rozdzynska-Kielbik, G. Dmytriv, and H. Ehrenberg, Li_4Ge_2B as a New Derivative of the Mo_2B_5 and Li_5Sn_2 Structure Types, *Acta Cryst. C*, 2016, **72**, p 561-565
42. V. Pavlyuk, G. Dmytriv, I. Tarasiuk, and H. Ehrenberg, $Li_9Al_4Sn_5$ as a New Ordered Superstructure of the $Li_{13}Sn_5$ Type, *Acta Cryst. C*, 2017, **73**, p 337-342
43. A. Stetskiv, I. Tarasiuk, R. Misztal and V. Pavlyuk, Thulium Nickel/Lithium Distannide, $TmNi_{1-x}Li_xSn_2$ (x = 0.035), *Acta Cryst. E*, 2013, **69**, p i76
44. P. Solokha, S. De Negri, M. Skrobanska, A. Saccone, V. Pavlyuk, and D. Proserpio, New Ternary Germanides $La_4Mg_5Ge_6$ and $La_4Mg_7Ge_6$: Crystal Structure and Chemical Bonding, *Inorg. Chem.*, 2012, **51**, p 207-214
45. E.I. Gladyhevskii, O.I. Bodak, Compounds with Structures of the AlB_2 Type in the System Ce-Ni-Si and in Related Systems, *Dopov. Akad. Nauk Ukr. RSR*, 1965, p 601-604
46. A.V. Morozkin, Y.D. Seropegin, and O.I. Bodak, Phase Equilibria in the Sm-{Ru, Rh }-{Si, Ge} Systems at 870, *J. Alloys Compd.*, 1996, **234**, p 143-150
47. V.V. Pavlyuk, I.M. Opaynych, O.I. Bodak, T. Palasinska, B. Rozdzynska, and H. Bala, Interaction of Components in the La-Ni-Zn System, *Polish Journal of Chemistry*, 1997, **71**, p 309-313
48. V.V. Pavlyuk, T.I. Yanson, O.I. Bodak, R. Cerny, R.E. Gladyshevskii, K. Yvon, J. Stepien Damm, Structure Refinement of Orthorhombic $MnAl_3$, *Acta Cryst. C*, 1995, 51, p 792-794